Ocean Engineering 267 (2023) 113248

Contents lists available at ScienceDirect

Ocean Engineering

journal homepage: www.elsevier.com/locate/oceaneng

Parametric study on the short-term extreme mooring tension of nylon rope for a point absorber

Sheng Xu [a], C. Guedes Soares [b,*]

[a] School of Naval Architecture and Ocean Engineering, Jiangsu University of Science and Technology, Zhenjiang, 212003, China
[b] Centre for Marine Technology and Ocean Engineering (CENTEC), Instituto Superior Técnico, Universidade de Lisboa, 1049-001, Lisboa, Portugal

ARTICLE INFO

Keywords:
Point absorber
Extreme mooring tension
Nylon mooring
Nonlinear axial stiffness

ABSTRACT

A series of 1:40 model tests are carried out to study the dynamic responses of a point absorber moored by three taut nylon ropes under irregular wave conditions. The experimental results are applied to calibrate a numerical model, and then the calibrated numerical model is applied to study the influence of pretension, mooring axial stiffness, current velocity and tidal range on extreme mooring tension under head sea wave conditions. Both the global maximum method and the average conditional exceedance rate method are applied to study extreme mooring tension based on fifty 3-h fully coupled analyses. The nonlinear strain-tension curve is used in numerical simulations to consider the material non-linearities of nylon rope. To discuss the influence of axial stiffness on extreme mooring tension, nonlinear strain-tension curves of a worked rope and a new rope are studied. The numerical simulations under three current profiles are conducted to study the influence of current velocity on extreme mooring tension. It is found that the influence of axial stiffness and current velocity on extreme mooring tension is significant, and the influence of current velocity on extreme mooring tension reduces with the increase of mooring pretension.

1. Introduction

The massive consumption of fossil energy causes air pollution and climate change. On the other hand, fossil resources are non-renewable and the reserves are limited, which leads to an energy crisis with continuous consumption of fossil energy. Consequently, renewable and sustainable energy has attracted great attention during the last decades. It is anticipated that the share of renewable energy in the total one could be as great as 63% in 2050 (Gielen et al., 2019). Solar photovoltaic (Sahu et al., 2016) and wind energy (Diaz and Guedes Soares, 2020) are key components of renewable energy, and they have been widely exploited in many countries. In addition to solar photovoltaic and wind energy, ocean wave energy shows many attractive features. It is pointed out that solar photovoltaic panels and wind turbines can only generate electricity up to 30% of the time, while wave energy converters (WECs) can absorb energy up to 90% of the time (Drew et al., 2009; Sheng, 2019). On the other hand, the wave energy resource is giant which is estimated at 2 TW (Thorpe, 1999). Furthermore, the energy density of ocean waves is the greatest among wind and solar and wave energy loss is small during wave transmission (Clément et al., 2002).

In this context, it is important to develop devices to harvest wave energy, and more than one thousand WECs have been developed (Czech and Bauer, 2012). Based on device size and installation direction relative to the incoming waves, WECs can be divided into different categories, i.e., point absorbers, attenuators and terminators (Falcão, 2010; Guedes Soares et al., 2012). Point absorbers are small-dimensional devices that are insensitive to the wave direction. Attenuators are designed with great length and are placed aligned with the incident wave crest (Falnes, 2007). Terminators are deployed with an orientation perpendicular to the dominant direction of wave travelling, and oscillating wave columns (OWCs) and overtopping devices are two well-known terminators. According to statistics, point absorbers are much more popular than the other two concepts, because point absorbers are easier to construct and maintain (López et al., 2013). One of the main issues in the development of WECs is the high capital cost (Castro-Santos et al., 2016). Because of this, multiple hybrid concepts which combine offshore structures and WECs are proposed to satisfy economic feasibility (Elginoz and Bas, 2017; Nguyen et al., 2020; Zhao et al., 2019; Gaspar et al., 2021). Among these hybrid concepts, the breakwater-integrated OWCs seem the most popular ones (Rezanejad et al., 2015; Arena et al., 2017; Kim et al., 2022).

The energy conversion performance of WECs is one of the greatest

* Corresponding author.
E-mail address: c.guedes.soares@centec.tecnico.ulisboa.pt (C. Guedes Soares).

https://doi.org/10.1016/j.oceaneng.2022.113248
Received 25 July 2022; Received in revised form 16 October 2022; Accepted 19 November 2022
Available online 2 December 2022

concerns during the design process. Several technologies are available to improve the energy harvesting performance of WECs, such as power take-off (PTO) control (Ahamed et al., 2020; Gaspar et al., 2016; Kong et al., 2019), optimization of WECs configuration (Kamarlouei et al., 2022; Li et al., 2022; Shih and Liu, 2022), adopting nonlinear stiffness (Schubert et al., 2022), adopting an adjustable draft system (Tan et al., 2022). In addition to these common strategies, developing floating devices is also an efficient way since the energy density of offshore waves is much greater than that of nearshore.

The mooring system which plays a role in keeping floating WECs on the station needs to be well-designed. The mooring design for WECs is different to that for offshore platforms since the operational manners and water depth of WECs are different to oil and gas platforms. Generally, WECs operate in water depths less than 100 m and it is easy to induce mooring snap loads under survival wave conditions which endanger system safety (Xu et al., 2020; Xu and Guedes Soares, 2020). Furthermore, the mooring system is related to the energy harvesting performance of WECs (Xu et al., 2021b) and mooring costs account for a large proportion of total investment in WEC systems (Fitzgerald, 2009). Consequently, it is a great challenge to design mooring systems for WECs (Xu et al., 2019b). It was pointed out that the catenary mooring system is not suitable for the application of WECs, while hybrid mooring concepts and synthetic fibre ropes are recommended (Xu et al., 2019b).

A series of model tests were conducted to study the influence of mooring rope material on hydrodynamic responses of a point absorber and mooring tensions, and it was shown that nylon rope is a favourable mooring material for a point absorber, which helps to improve energy harvesting performance and reduce mooring tension (Xu et al., 2021b, 2021c). It is difficult to simulate the mechanical properties of synthetic fibre ropes due to viscoelastic and viscoplastic characteristics, and most studies assume that the axial stiffnesses of synthetic fibre ropes are liner. However, it was pointed out that the non-linearities of synthetic fibre rope material have a significant influence on mooring tensions and motion responses of WECs (Bhinder et al., 2015). Taking viscoelastic and viscoplastic properties into consideration in a floating structure-mooring system fully coupled analysis is a cumbersome work, and two alternative approaches are available, i.e., the nonlinear stiffness method (Bhinder et al., 2015; Li and Choung, 2021) and dynamic stiffness method (Depalo et al., 2022; Liu et al., 2014; Xu et al., 2021e). However, an iteration procedure is needed during the implementation of the dynamic stiffness method (Depalo et al., 2022; Pham et al., 2019). In other words, the nonlinear stiffness method is an easier approach than the dynamic stiffness approach.

The ultimate limit states design is one of the crucial steps during the mooring design process, which makes sure that the mooring line has enough strength to withstand extreme environmental load during the service life. In other words, the extreme mooring tension needs to be predicted accurately. Various probability distribution models are available for extreme mooring analysis, such as Gumbel distribution, Weibull distribution, generalized extreme value (GEV) distribution, peak-over-threshold (POT) method and the average conditional exceedance rate (ACER) method (Ambühl et al., 2014; Cheng et al., 2017; Naess and Gaidai, 2009; Pickands, 1975; Xu et al., 2019a). Among these methods, the global maximum method which applies the Gumbel method to fit the maximum values of each simulation is considered a benchmark in extreme value analysis (Stanisic et al., 2018; Xu et al., 2019a). However, it was pointed out that the global maximum method is time-consuming, while the extrapolation approach based on the ACER method is much more efficient and accurate enough (Xu et al., 2019a, 2021a; Xu and Guedes Soares, 2021a; Zhao et al., 2021).

After an extensive review of current studies, it is concluded that nylon rope is a favourable material for WEC moorings, and the nonlinear mechanics need to be considered for predicting accurate enough mooring tensions. However, the extreme mooring tension analysis with material non-linearities considered is rare. Furthermore, WECs operate in shallow water, consequently, the influence of tidal range on WECs dynamics and mooring tensions needs to be investigated. The paper is organized as follows. In Sect. 2, the introduction to a point absorber and its mooring system is given. Sec. 3 presents methodologies for coupled dynamic analysis and extreme mooring tension analysis (global maximum method and ACER method). In Sect. 4, the validation of the numerical model is conducted in 4.1, and then the influence of mooring axial stiffness, current velocity and tidal range on extreme mooring tension is investigated. Then the influence of time duration and number of simulations on the performance of the ACER method for extreme mooring tension analysis based on the extrapolation approach is discussed. Finally, the conclusions of the paper are then given in Sect. 5.

2. Model description and experimental set-up

2.1. Point absorber and mooring system

A cylinder with a bottom cone is designed for wave energy harvesting, and Fig. 1 shows the schematic of the 1:40 WEC model used in hydrodynamic model tests. It is seen that the total height of this model is 50 cm, i.e., the total height of WEC in full scale is 20 m. As seen in Fig. 1, three pulleys which are used to connect mooring ropes are equally arranged on the WEC and the azimuth angle between two pulleys is 120°. The main parameters of the WEC model are shown in Table 1, where Φ denotes the diameter, δ is the free draft (without mooring installed), Δ is

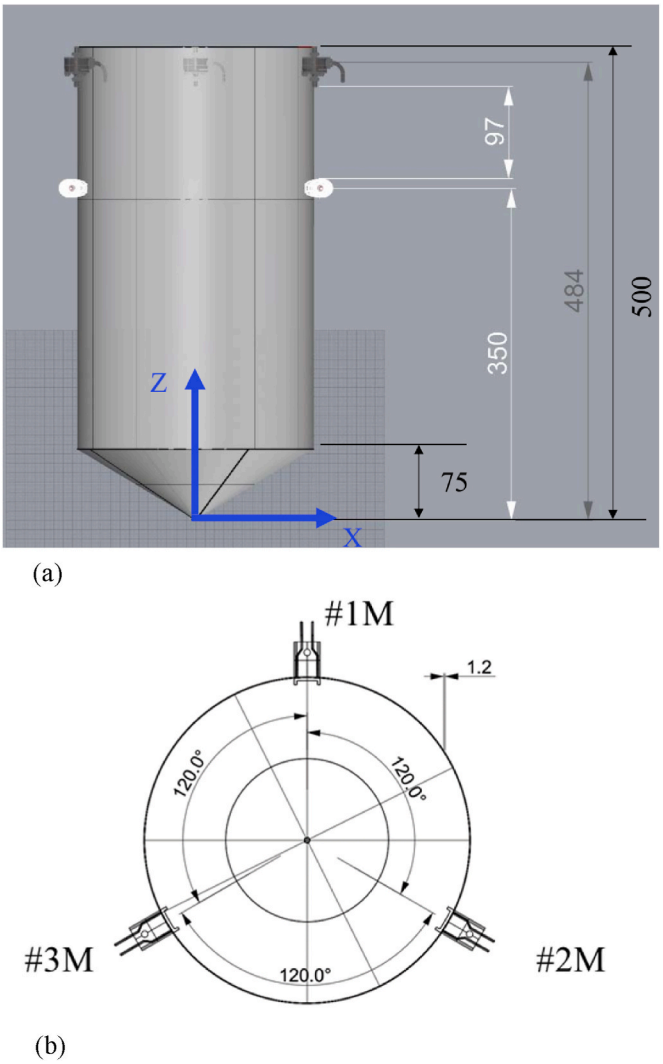

Fig. 1. Schematic of 1:40 WEC model used in model tests (unit: mm) (a) side view (b) top view.

Table 1
Main parameters of point absorber model.

Parameters	Value	Parameters	Value
Φ(mm)	250	Y_{CoG}(mm)	0
H(mm)	500	Z_{CoG}(mm)	163
δ(mm)	300	Rxx(mm)	140
Δ(kg)	12.27	Ryy(mm)	140
X_{CoG}(mm)	0	Rzz(mm)	110

the displacement, the gravity centre locates in the centre of X–Y plane and its height is 163 mm (the baseline is in the bottom of the model, as shown in Fig. 1), Rxx, Ryy, Rzz are the gyration radius around X, Y, and Z axis respectively.

Following the research of Yang et al. (2020, 2018), a steel heave plate and a linear spring are used to simulate the damping and stiffness of the PTO system, as seen in Fig. 2. The length and width of the heave plate are 10 cm, and its thickness is 1 mm. The stiffness of linear spring is 29.22 N/m. To install this simplified PTO system, a 50 cm connection bar is used to fix the heave plate to the WEC, and a 92.86 cm wire rope is applied to connect the linear spring and the heave plate. The diameter of the wire is 3.5 mm and its mass per unit length in air is 0.108 kg (with the clamps considered, as seen in Fig. 2(b)).

As shown in Fig. 3, the mooring system consists of three taut nylon ropes, and the azimuth angle between two mooring ropes is 120°. In this study, only the head sea wave condition is studied, consequently, the #1 M mooring is the most loaded one. As seen in Fig. 2 (b), the WEC is moored by taut ropes with the help of clamps, and the length of the clamp is 55 mm. Four load sensors were used during model tests, including one installed on the floor, and three installed on the top of each hook, which is used to connect the mooring rope to the WEC. The length of nylon mooring ropes is 2.5632 m, the nominal diameter is 3 mm and the mass per unit length in air is 5.02 g/m. The static tension-

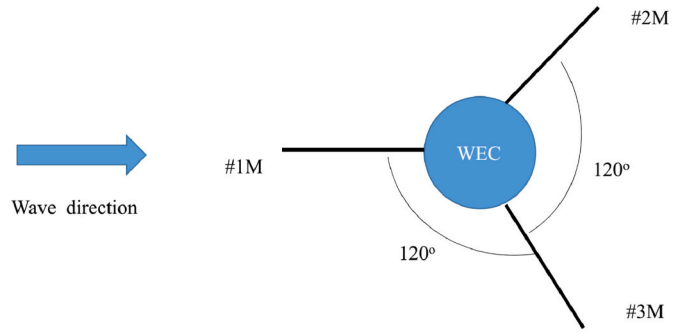

Fig. 3. Schematic of arrangement of mooring lines.

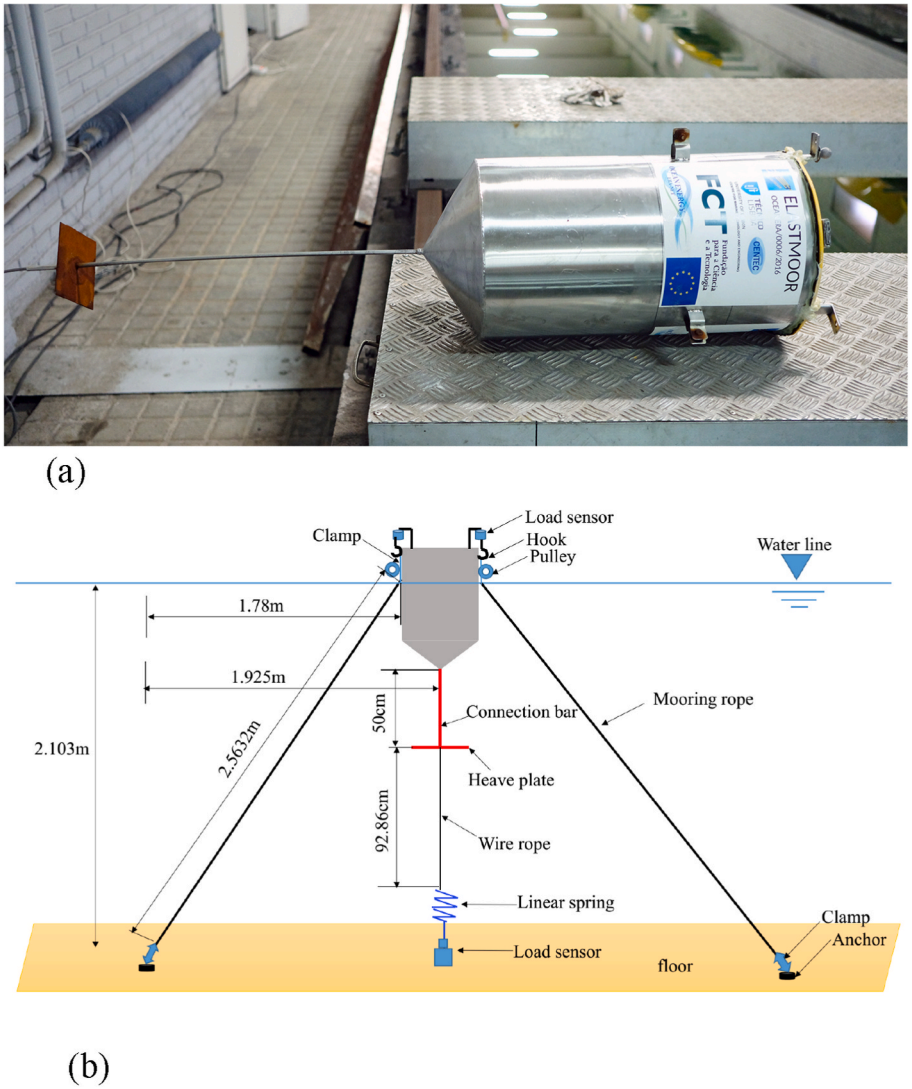

Fig. 2. Point absorber and PTO system model (a) 1:40 model of point absorber (b) schematic of WEC and PTO system.

elongation curve of nylon rope was measured (Xu et al., 2021d, 2021e), and the relation between them is given based on the experimental data:

$$T = 0.025 + 3.719\varepsilon + 60.535\varepsilon^2 + 58.341\varepsilon^3 \quad (1)$$

where ε is the strain, T is the tension in KN. The axial stiffness is calculated as EA $= \Delta T/\Delta\varepsilon$, and the nonlinear axial stiffness curve can be obtained once the tension versus strain curve is known. Then the nonlinear stiffness-strain curve acted as input in the commercial software ANSYS AQWA to simulate dynamic responses of the WEC and mooring tension (ANSYS Inc, 2015).

The designed pretension of the mooring rope was 20 N, however, it is difficult to adjust the pretension of these different mooring ropes to be identical. Part of the reason is that a great pretension was adopted in the model tests, and the system was very stiff. As a consequence, it is a big challenge to adjust the pretension in water. Besides, the viscoelastic and viscoplastic characteristics of nylon ropes also give rise to difficulties in adjusting mooring pretension. Finally, after slightly adjusting, the pretension of #1 M, #2 M and #3 M was 20.21 N, 20.18 N and 20.86 N respectively.

2.2. Experimental set-up

The 1:40 hydrodynamic model tests have been carried out in the towing tank of ETSIN (Universidad Politécnica de Madrid), where the length, width and depth of the tank are 96 m, 3.8 m and 2.103 m respectively. The model tests were conducted according to the Froude similitude rule, and all the experimental data are converted to full scale in this study.

Fig. 4 shows the sketch of the experimental set-up, where it is seen that the model was installed 35 m away from the wave paddle to keep enough space between the model and the wave dissipating beach to reduce the influence of the reflection wave on system dynamics. Three wave probes were used to measure wave elevations, the positions of WP1 and WP2 can be found in Fig. 2, and WP2 was placed 1.2 m to the starboard of WEC. An optical tracking system was used to measure six degrees of freedom motion responses of the WEC. As shown in Fig. 1(b), three submersible load cells with the capacities 0–50 N were installed on the top frame to record the mooring tension time series. The sampling frequency of all sensors was set to 50 Hz. The irregular wave model test was conducted, and the irregular wave was modelled by the JONSWAP spectrum, the wave peak period was 1.11 s and the significant wave height was 0.05 m (7.02 s and 2 m in full scale).

3. Analysis methodologies

3.1. Coupled dynamic analysis

The governing equation of floating structure is expressed as (ANSYS Inc, 2015):

$$(\mathbf{M} + \mathbf{A}_\infty)\ddot{\mathbf{x}} + \mathbf{C}_1\dot{\mathbf{x}} + \mathbf{C}_2\mathbf{f}(\dot{\mathbf{x}}) + \mathbf{K}\mathbf{x} + \int_0^t \mathbf{h}(\mathbf{t}-\tau)\dot{\mathbf{x}}(\tau)d\tau = \mathbf{q}(\mathbf{t}, \mathbf{x}, \dot{\mathbf{x}}) \quad (2)$$

where $\mathbf{M}$ is the body mass matrix, $\mathbf{A}_\infty$ is the added mass matrix when the frequency closes to infinite, $\mathbf{C}_1$ is the linear damping matrix, $\mathbf{C}_2$ is the quadratic damping matrix, $\mathbf{K}$ is the stiffness matrix, $\mathbf{f}$ is the vector function, the element is given by:

$$f_i = \dot{x}_i|\dot{x}_i| \quad (3)$$

$\mathbf{h}(\tau)$ is the retardation function, which is computed by the frequency-dependent added mass and damping transformation:

$$\mathbf{h}(\tau) = \frac{1}{\pi}\int_0^\infty [\mathbf{c}(\omega)\cos\omega\tau - \omega\mathbf{a}(\omega)\sin\omega\tau]\mathrm{d}\omega \quad (4)$$

where $\mathbf{a}(\omega) = \mathbf{A}(\omega) - \mathbf{A}_\infty$, $\mathbf{c}(\omega) = \mathbf{C}(\omega) - \mathbf{C}_\infty$, $\mathbf{C}_\infty$ is the potential damping matrix when the frequency closes to infinite, where

$$\mathbf{a}(\omega) = \frac{1}{\pi}cv\int_{-\infty}^{\infty}\frac{[\mathbf{C}(f)]}{f(f-\omega)}df \quad (5)$$

where cv denotes the Cauchy principal value.

The right side of Eq. (2) is the excitation force vector, which is expressed as:

$$\mathbf{q}(\mathbf{t}, \mathbf{x}, \dot{\mathbf{x}}) = \mathbf{F}^1 + \mathbf{F}^2 + \mathbf{F}^c + \mathbf{F}^d + \mathbf{F}^m \quad (6)$$

where $\mathbf{F}^1$ and $\mathbf{F}^2$ are the first-order and second-order wave forces respectively, $\mathbf{F}^c$ is the current drag force, $\mathbf{F}^d$ is the wave drift damping force, $\mathbf{F}^m$ is the mooring tensions.

The two stages strategy is applied to solve the governing equation (ANSYS Inc, 2015), the global equation of motion responses in the time domain is defined as:

$$(\mathbf{M} + \mathbf{A}_\infty)\ddot{\mathbf{x}} = \mathbf{q}_t \quad (7)$$

where

$$\mathbf{q}_t = \mathbf{q}(t) - \mathbf{C}_1\dot{\mathbf{x}} - \mathbf{C}_2\mathbf{f}(\dot{\mathbf{x}}(t)) - \mathbf{K}\mathbf{x}(t) - \int_0^t \mathbf{h}(\mathbf{t}-\tau)\dot{\mathbf{x}}(\tau)d\tau \quad (8)$$

First, the total excitation force $\mathbf{q}(t)$ is calculated at a known time,

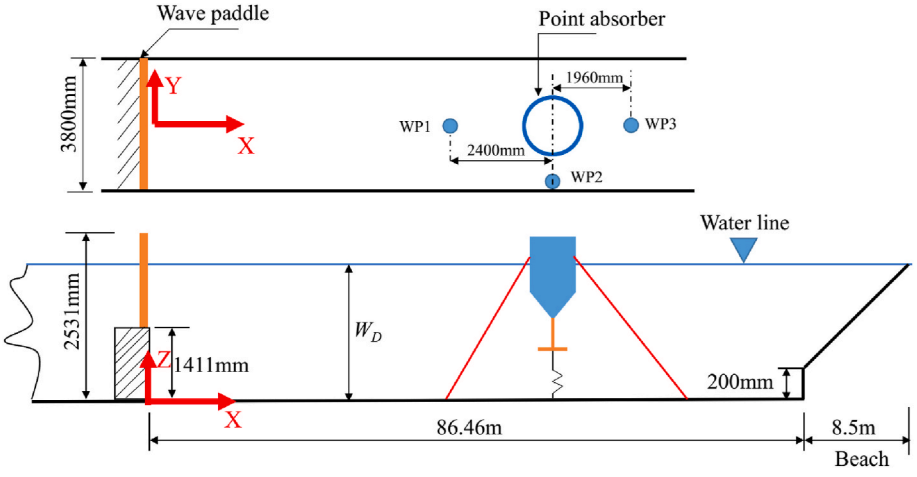

Fig. 4. Experimental set-up.

position and velocity:

$$\mathbf{q}_t(t) = \mathbf{f}(t, \mathbf{x}(t), \mathbf{v}(t)) \tag{9}$$

The acceleration is then solved by substituting Eq. (9) to Eq. (7), and the predicted velocity and position at time $t + dt$ is given as:

$$\mathbf{v}^*(t+dt) = \mathbf{v}(t) + \ddot{\mathbf{x}}(t)dt \tag{10}$$

$$\mathbf{x}^*(t+dt) = \mathbf{x}(t) + \mathbf{v}(t)dt + \ddot{\mathbf{x}}(t)\frac{dt^2}{2} \tag{11}$$

where the superscript * indicates intermediate results in the predictor-corrector algorithm.

The total applied force at $t + dt$ is estimated as:

$$\mathbf{q}_t^*(t+dt) = \mathbf{f}(t+dt, \mathbf{x}^*(t+dt), \mathbf{v}^*(t+dt)) \tag{12}$$

The estimated acceleration at $t + dt$ is solved by substituting Eq. (12) to Eq. (7), then the corrected velocity and position is the calculated at time $t + dt$ by using Taylor's theorem:

$$\mathbf{v}^*(t+dt) = \mathbf{v}(t) + \frac{\ddot{\mathbf{x}}(t) + \ddot{\mathbf{x}}^*(t+dt)}{2}dt \tag{13}$$

$$\mathbf{x}^*(t+dt) = \mathbf{x}(t) + \mathbf{v}(t)dt + \frac{2\ddot{\mathbf{x}}(t) + \ddot{\mathbf{x}}^*(t+dt)}{6}dt^2 \tag{14}$$

3.2. Extreme value analysis

3.2.1. Global maximum method

By noticing that the extreme peaks will approach a Gumbel distribution, this model is widely used in predicting structural extreme responses. The cumulative distribution function (CDF) of Gumbel distribution is:

$$F(x;\mu,\sigma) = \exp\left[-\exp\left(-\frac{x-\mu}{\sigma}\right)\right] \tag{15}$$

where μ_l and σ_l are the location factor and scale factor respectively, and these two parameters can be easily fitted by L-moments method (Bílková, 2014; Xu et al., 2019a).

The most probable maximum extreme (MPME) value, which is the mode value has a 63.2% chance to be exceeded, and this value is calculated according to

$$x_{\mathrm{mp}} = \mu - \sigma\ln\{-\ln(F(1-0.632))) = \mu \tag{16}$$

3.2.2. ACER method

The ACER method was developed based on the cascade of conditional approximation (Naess and Gaidai, 2009). By assuming that all the peaks X_j are statistically independent, the $P(\eta) = \mathrm{Prob}(M_N \leq \eta)$ is approximated as (Naess and Gaidai, 2009):

$$P(\eta) \approx \prod_{j=1}^{N} P(X_j \leq \eta) \tag{17}$$

where $M_N = \max\{X_j; j = 1, \ldots, N\}$.

The conditional exceedance probability is defined as:

$$\alpha_{kj} = \mathrm{Prob}\{X_j > \eta \,|X_{j-k+1} \leq \eta, \ldots, X_{j-1} \leq \eta\} \tag{18}$$

where α_{kj} denotes exceedance probability conditional on k-1 previous non-exceedances.

Assuming that the conditional exceedances events are independent and follow a Poisson process, the extreme value distribution can be approximated as:

$$P_k(\eta) \approx \exp\left(-\sum_{j=k}^{N}\alpha_{kj}(\eta)\right) \tag{19}$$

where $\sum_{j=k}^{N}\alpha_{kj}(\eta)$ is the independent expected effective number of exceedances provided by conditioning on k-1 previous observations.

The conditional average exceedance rate (AER) is defined as:

$$\bar{\varepsilon}_k = \frac{1}{N-k+1}\sum_{j=k}^{N}\alpha_{kj}(\eta), k = 1, 2, \ldots. \tag{20}$$

For both stationary and non-stationary time series, the sample estimate of ACER would be:

$$\widehat{\varepsilon}_k(\eta) = \frac{1}{M}\sum_{m=1}^{M}\widehat{\varepsilon}_k^{(m)}(\eta) \tag{21}$$

where M is the number of samples, index (m) refers to the realization no. m.

Assuming the samples are independent, the 95% confidence interval CI for ACER is given as:

$$\mathrm{CI}^{\pm}(\eta) = \widehat{\varepsilon}_k(\eta) \pm \frac{1.96\widehat{s}_k(\eta)}{\sqrt{M}} \tag{22}$$

where, $\widehat{s}_k(\eta)$ is the standard deviation of $\widehat{\varepsilon}_k(\eta)$:

$$\widehat{s}_k(\eta)^2 = \frac{1}{M-1}\sum_{m=1}^{M}\left(\widehat{\varepsilon}_k^{(m)}(\eta) - \widehat{\varepsilon}_k(\eta)\right)^2 \tag{23}$$

Assuming the mean exceedance rate in the tail is dominated by an exponential function, it is approximated as (Naess and Gaidai, 2009):

$$\varepsilon_k(\eta) \approx q_k(\eta)\exp\{-a_k(\eta - b_k)^{c_k}\} \;\; \eta \geq \eta_1 \tag{24}$$

where a_k, b_k, c_k and q_k are the parameters related to k, η_1 equals the threshold.

The parameters a, b, c and q are determined by minimizing the following mean square error function with respect to all four arguments:

$$F(a,b,c,q) = \sum_{j=1}^{R} w_j\left|\log\widehat{\varepsilon}_k(\eta_j) - \log q + a(\eta_j - b)^c\right|^2 \tag{25}$$

where $\eta_1 < \ldots < \eta_R$ denotes the levels where ACER function has been estimated, w_j denotes a weight factor, it is given as:

$$w_j = \left(\log C^+(\eta_j) - \log C^-(\eta_j)\right)^{-\theta} \tag{26}$$

$\theta = 1$ or 2, in this study, $\theta = 2$ is used. The parameters in Eq. (16) can then be solved by Levenberg–Marquardt method by simplifying four parameters into two (Saha et al., 2014).

The relation between CDF of peak values and extreme values is expressed as (Ochi, 1981; Razola et al., 2016):

$$F^n(x) = F_e(x) \tag{27}$$

where n is the number of peaks, $F_e(x)$ is the CDF of extreme responses, $F(x)$ is the CDF of peak responses. The extreme value with an exceedance probability α is expressed as:

$$P[x_e > x] = \alpha = 1 - F_e(x) = 1 - F^n(x) \tag{28}$$

Under the assumption that the $\alpha < 1$, by applying the Taylor expansion, Eq. (19) can be rewritten as (Razola et al., 2016):

$$1 - F(x) = \frac{\alpha}{n} \tag{29}$$

The most probable largest value for a sample of independent and identically distributed (IID) data can be estimated by solving the following equation (Ochi, 1981):

$$1 - F(x) = \frac{1}{n} \tag{30}$$

As stated above, n is the number of peaks of the concerned period (typically 3-h for offshore engineering). If the extrapolation method is applied, the n can be calculated as:

$$n = \upsilon_p R \tag{31}$$

where R is the return period, υ_p is the expected rate of occurrence of peaks, which is approximated:

$$\upsilon_p = \frac{n_s}{T_s} \tag{32}$$

where n_s is the number of peaks during the overserved period T_s. By invoking Eq. (23) into Eq. (22), the n is expressed as:

$$n = R\frac{n_s}{T_s} \tag{33}$$

4. Numerical study on the short-term extreme surge motions and mooring tensions

In this section, the influence of pretension, axial stiffness of mooring rope and current velocity on the short-term extreme responses of the WEC and mooring lines are numerically analysed. Before conducting numerical simulations, the accuracy of the numerical model is validated by the experimental data.

4.1. Validation of the numerical model

The fully coupled dynamic analysis was conducted in AQWA (ANSYS Inc, 2015). As can be seen in Fig. 2(b), the top end of the mooring rope is connected to a vertical frame through a pulley during the model tests, in other words, the mooring loads are always perpendicular to the horizontal section plane of the WEC, which is difficult to be considered in numerical simulations. As a consequence, the pulleys and the frames are neglected during the numerical simulations, which will give rise to the difference in the restoring force between the numerical and experimental mooring systems, especially for the heave and pitch modes. Since a relatively large pretension was used during the experimental test, correspondingly, the dynamic differences between the numerical and experimental models due to the simplified numerical model could be enlarged. The mooring pretension of the numerical model is adjusted to be the same as the design pretension of the model tests, i.e., 1280 KN (change to full scale based on Froude's model law). The hydrodynamic coefficients of the WEC as well as the mooring rope are adjusted during the calibration process to make the numerical results as close as the measured ones.

To check the accuracy of the numerical model, the simulated results are compared with the measured ones. The three main motion responses of WEC in the head sea wave condition are shown in Fig. 9, where only 100 s data are plotted to show the results clearly. Furthermore, spectral analysis is conducted to study the components of motion responses. It is observed that the numerical results are satisfied, and the trend of simulated motion response time series is generally is consistent with the corresponding measured ones despite the difference in peak values. The greatest differences are found in the pitch and heave motion responses. It is explained that the top connection component of these two models is different (as seen in Figs. 2 and 5), the numerical model neglects pulleys and frames which makes the influence of moorings on the WEC motions different to that of the experimental one, especially for pitch and heave. Compared with the experimental model, the pitch moment from the mooring is reduced in numerical simulation. As a result, the numerical model underestimates the pitch motion responses. Since the surge motion is coupled with the surge, the reduction of pitch motion response will give rise to a smaller surge motion response, and this phenomenon

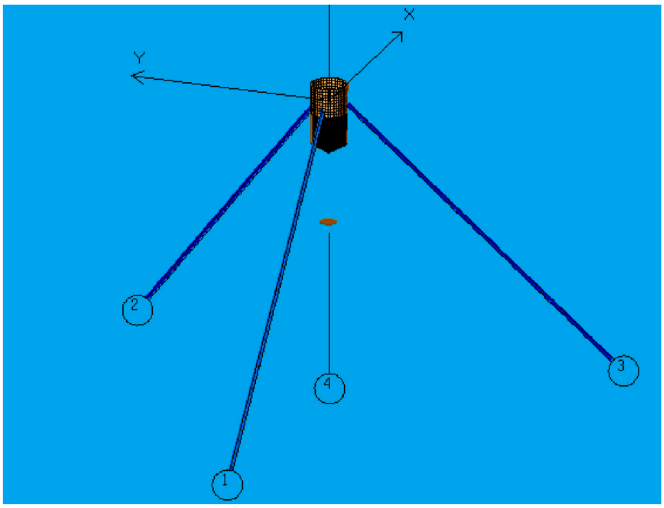

Fig. 5. Numerical model of WEC moored by three taut mooring ropes.

can be found in Fig. 6(b) and (f).

According to the spectral densities of these three motion responses, it is found that wave frequency plays a dominant role in determining the components of motion responses. The peaks which occur close to the wave peak period are found in the motion spectral densities. In addition to the wave peak period, the motion resonance also affects the property of motion responses. In Fig. 6 (b), (d) and (f), it is observed that the experimental spectral peak that appears in the vicinity of the corresponding natural period of motion response is smaller than that near the wave peak period. In Fig. 6 (d), it is observed that the numerical spectral peak period due to heave resonance is different to the experimental one. The reason is that the mooring connection type between these two models is different, which leads to the difference in the natural heave period. Furthermore, a disk element is applied to simulate the heave plate by setting the area between them to be identical. In other words, the PTO damping is not calibrated in the numerical simulations, and the uncertainties of the PTO system also contribute to the dynamic differences between the numerical and experimental results. Third, the nonlinearities of the WEC system are observed from the model tests, including overtopping and vortex-induced motion, which cannot be considered by the AQWA. Nevertheless, the uncertainty of the mooring system is the main factor that leads to the difference in dynamic responses between these two systems, since the motion responses of the WEC are strongly associated with the mooring system, and the influence of mooring frame and viscoelastic properties of mooring rope (which are neglected by the numerical model) on mooring dynamics and the WEC motions will be enlarged due to the large mooring pretension.

To check the accuracy of the numerical model clearly, the statistics of WEC motion responses are concluded in Table 2, where Max means the maximum, Min indicates the minimum and Std is the standard deviation. It is found that the numerical results are in good agreement with the measured ones, especially for the surge motion response. The maximum difference is found in the minimum heave and pitch response, and the reason has been given above, and will not be repeated here.

The mooring tensions and mooring tension spectral densities are plotted in Figs. 7 and 8, since the #2 M and #3 M are symmetrically arranged, only the results of #1 M and #2 M are presented. According to the comparisons of the mooring tension time series, it is observed that the numerical results match well with the experimental data, except for the minimum mooring tension of the #1 M. The spectral analysis is then conducted and the results are presented in Figs. 7 (b) and Fig. 8(b), where it is seen that the configurations of mooring tension spectral densities between these two models are similar. It is found that a dominated spectral peak occurs near the wave peak period. However, the experimental motion resonances show a more significant influence

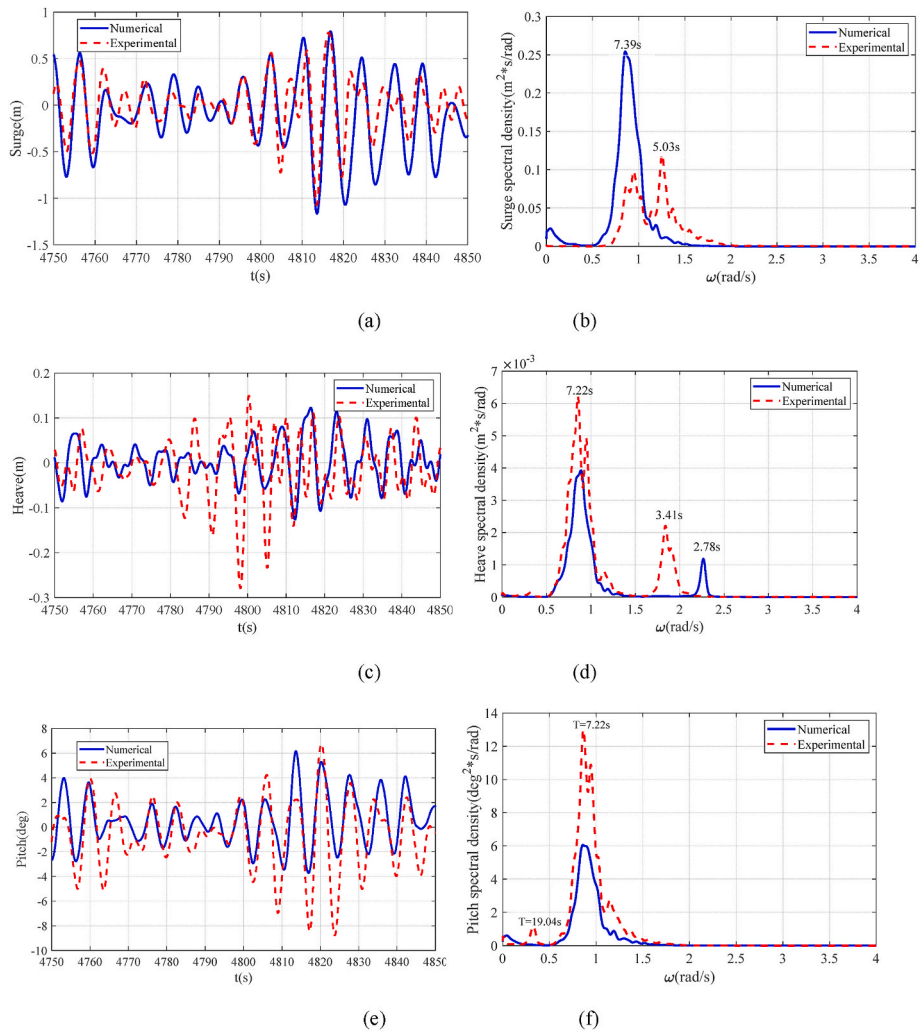

Fig. 6. Comparisons of three main motion responses of WEC (a) Surge response time series (b) Surge spectra (c) Heave motion response time (d) Heave spectra (e) Pitch motion response time (f) Pitch spectra.

Table 2
Statistics of motion responses.

	Statics	Experimental	Numerical
Surge(m)	Max	0.90	0.89
	Min	−1.11	−1.54
	Mean	−0.01	−0.04
	Std	0.21	0.26
Heave(m)	Max	0.18	0.16
	Min	−0.31	−0.15
	Mean	−0.01	0.00
	Std	0.05	0.03
Pitch(deg)	Max	7.00	7.70
	Min	−9.20	−4.26
	Mean	−0.48	0.20
	Std	1.88	1.33

on mooring tensions compared with the numerical results. It is seen that in the experimental data, the surge, heave and pitch resonances exhibit more or fewer effects on mooring tensions, while only the effect of heave resonance on mooring tension is found in the numerical data.

The statistics of mooring tensions are summarized in Table 3, where it is observed that the numerical model almost presents accurate estimations of maximum mooring tensions. The largest difference is found in the minimum tension of #1 M mooring, and the reason has been given in the previous discussions. However, generally, the maximum mooring tension is the most concerning, it is seen the difference in maximum tension between experimental and numerical models is 8% and 1% for #1 M and #2 M respectively.

It is found that the pitch motion responses of the WEC and the minimum tension of the #1 M is not well predicted by the numerical model due to uncertainties of the numerical model stated above. However, it is seen that the maximum mooring tension is predicted accurately. With respect to the fact that the maximum mooring tension is the primary concern of this study, the numerical model is deemed acceptable for extreme mooring tension analysis.

4.2. Study cases

As seen in the experimental part, a scaled-down nylon rope was applied, which indicates that the axial stiffness of nylon rope at full scale will be overestimated considerably. In other words, considerable errors will be introduced if the experimental data are used to predict dynamic responses of full-scale systems. However, the main purpose of the experimental study of this work is to check the accuracy of the numerical model rather than to predict the dynamics of full scale. In the following study, the real axial stiffness of a full-scale nylon rope is considered in the calibrated numerical model. A double braided nylon rope is studied in this work, the nominal diameter is 128 mm, the wet break strength is 3759 KN and the mass per unit length is 1.025 kg/m (Lankhorst Offshore). In the numerical simulations, the parameters of the new rope

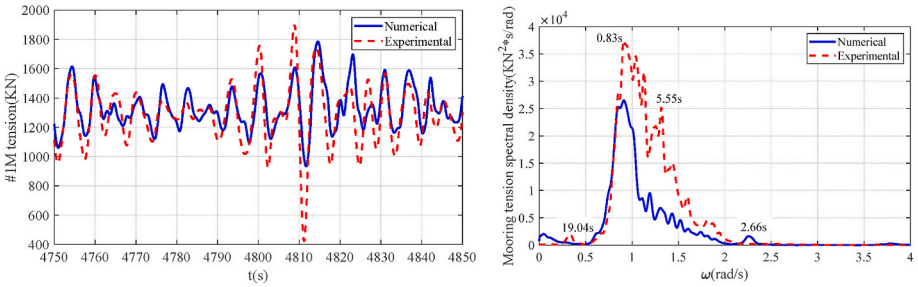

Fig. 7. Comparisons of #1 mooring tensions in random waves (a) #1 M tension time series (b) #1 M tension spectra.

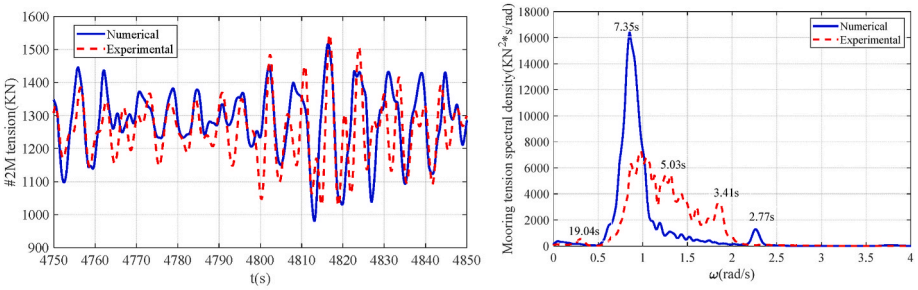

Fig. 8. Comparisons of #2 mooring tensions in random waves (a) #2 M tension time series (b) #2 M tension spectra.

Table 3
Statistics of mooring tensions.

	Statics	Experimental	Numerical
#1 M(KN)	Max	2046.46	1881.33
	Min	323.63	897.06
	Mean	1286.91	1311.22
	Std	144.58	107.23
#2 M(KN)	Max	1546.60	1562.72
	Min	944.87	885.26
	Mean	1259.87	1290.98
	Std	70.95	68.91

and the worked rope are identical, except for the axial stiffness. The Jonswap spectrum is used to simulate irregular waves, the significant wave height is 8 m, and the wave peak period is 13 s, which is the most frequent large wave condition of the assumed target sea field (west Portuguese coast, 39 N, 9.5 W (Xu and Guedes Soares, 2021b)). The mooring arrangement, mooring length and water depth are identical to the model test (change to full scale based on the Froude's model law and model scale is 1:40).

The influence of mooring pretension, current velocity and tidal range on the 3-h short-term extreme mooring tension are studied. Furthermore, the influence of the time duration and number of simulations on the performance of ACER method based on the extrapolation approach is also discussed. The pretension is set by adjusting the mooring radius without changing the mooring length. The PTO system is neglected in the following study to remove the uncertainties of the PTO system in the numerical simulations since the extreme mooring tension is the main concern of this work.

4.2.1. *Influence of mooring axial stiffness on short-term responses*

The tension-strain curves of a new and worked wet double-braided nylon rope are shown in Fig. 9, where it is found there is a great difference in the axial stiffness between these two ropes. The influence of axial stiffness on extreme mooring tension is discussed under two pretensions, and the pretension is set by adjusting the mooring radius, i.e., $R = 81$ m (the pretension of the worked and the new rope is 372 and 91 KN) and $R = 77$ m (the pretension of the worked and the new rope is 206 and 63 KN) respectively. Under head sea wave conditions, the #1 mooring is the most loaded one and the extreme tension of this cable will be studied in the following work.

The 3-h fully coupled dynamic analysis is carried out by the calibrated numerical model, and the nonlinear axial stiffness is simulated by a polynomial function. Mooring tension time series of the new and the worked #1 M when $R = 81$ m are plotted in Fig. 10, where it is found that the influence of axial stiffness on mooring tension is significant. The mooring tension of the worked rope is much greater than the new one since the new rope is much softer than the worked one, as seen in Fig. 9.

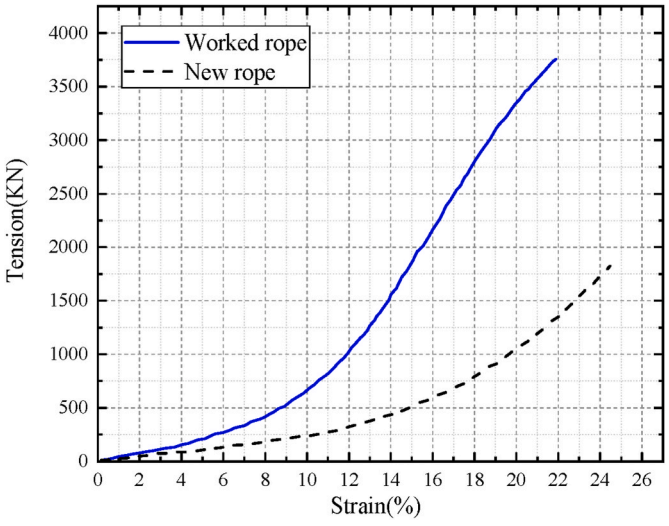

Fig. 9. Tension-strain curve of a double braided nylon rope (Lankhorst Offshore).

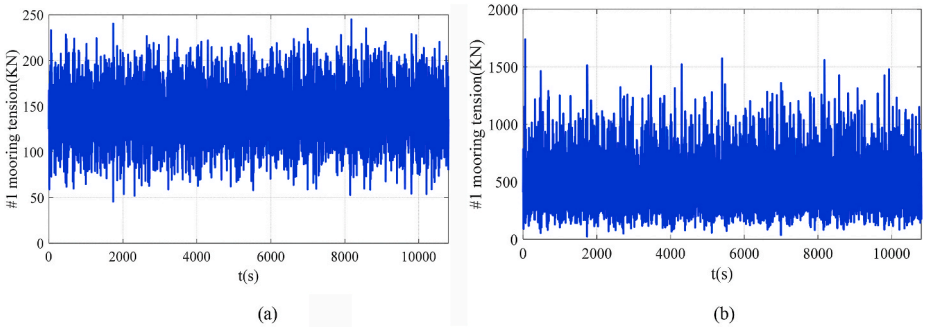

Fig. 10. #1 Mooring tension time series, $R = 81$ m (a) the new rope (b) the worked rope.

The 3-h fully coupled dynamic analysis is then repeated 50 times with different wave seeds to take random wave elevations into considerations. The maximum tension of each simulation is extracted and used to fit parameters of Gumbel distribution by the L-moment method (Bílková, 2014), and the Q-Q plots of the Gumbel model for extreme tension analysis of #1 mooring under $R = 81$ m are plotted in Fig. 11, where it can be found that the parameters of Gumbel models are well fitted. It indicates that the Gumbel model can present good estimations of extreme mooring tension by applying Eq. (7). In addition to the Gumbel method, the ACER method is also applied to study short-term extreme mooring tension based on fifty 3-h numerical simulations, and the average exceedance rates of mooring tension with a degree of conditioning equal to three are plotted in Fig. 12. It is seen that the empirical exceedance rates are well fitted by the numerical one, which implies that the ACER method can present accurate enough estimations to extreme mooring tensions.

The Gumbel method and ACER method are then applied to study the extreme mooring tension when $R = 77$ m, and the estimated extreme mooring tensions under these two mooring radiuses are summarized in Table 4. It can be seen that the ACER method shows excellent performance in predicting extreme mooring tension, the difference between Gumbel results and ACER results is smaller than 2% for all studied cases. The axial stiffness shows a remarkable influence on extreme mooring tension, it is observed that the extreme mooring tension of the worked rope is six times the one of the new rope when $R = 77$ m. Moreover, it is found that the influence of axial stiffness on extreme mooring tension increases with the pretension. For instance, the extreme mooring tension of the worked rope is around seven times that of the new rope when $R =$ 81 m.

4.2.2. *Influence of current velocity on short-term extreme mooring tension*

The axial stiffness of the worked rope is used in the following study. In the current section, the influence of current velocity on extreme mooring tension is investigated, and a linear current profile is used (DNV GL, 2017). In this study, three current cases are investigated for each mooring tension under three mooring radius cases, i.e., $R = 77$, 81 and 85 m (the pretension of worked rope is 623 KN under this mooring radius). The current velocity at the still water level is set as 0 m/s, 0.5 m/s, 2 m/s respectively.

The #1 mooring tension time series under different wave conditions when $R = 77$ m are shown in Fig. 13, and the results of $R = 81$ m are not plotted. It is seen that the influence of current velocity on mooring tensions is considerable, i.e., the mooring tension increases with the current velocity. The reason is that the hydrodynamic forces on the WEC and mooring lines increase nonlinearly with the current velocity.

The 3-h numerical simulations are then repeated fifty times for extreme mooring tension analysis, and the maximum #1 mooring tensions in each simulation acted as samples for fitting parameters of Gumbel distribution. The Q-Q plot is conducted to check the accuracy of parameters fitting, as shown in Fig. 14, where it is seen that the parameters of the Gumbel model are well fitted. The ACER method is applied to fit the averaged conditional exceedance rates (three degrees of conditioning) of fifty 3-h mooring tensions, and the results are shown in Fig. 15, where a good agreement between the fitted and empirical exceedance probability of measured data can be found. It implies that the ACER method can present precise estimations of extreme mooring tension.

The 3-h short-term extreme mooring tensions estimated by different methods under these three pretension cases are shown in Table 5. It is seen that the results of ACER method are in good agreement with Gumbel's results, which implies that the ACER method is a favourable approach in extreme mooring tension analysis. The current velocity shows a noticeable influence on extreme mooring tension, it is seen that the extreme mooring tension increases gradually with current velocity. Furthermore, it is found that the influence of current velocity on extreme mooring tension decreases with the increase of pretension. For instance, the extreme mooring tension under $V_c = 2$ m/s is 68% greater than that under $V_c = 0$ m/s when $R = 77$ m, while this value is 45% and 32% for the cases $R = 81$ m and $R = 85$ m respectively. It is explained that the restoring force of mooring systems increases with mooring pretension,

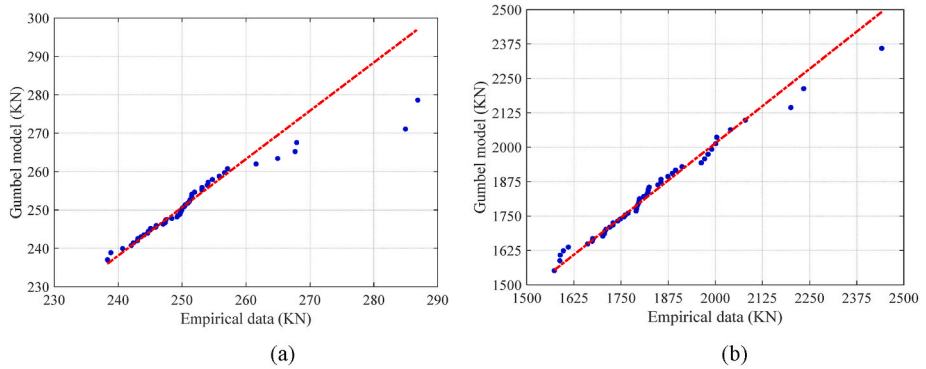

Fig. 11. Q-Q plot of Gumbel model for extreme tension analysis of #1 mooring, $R = 81$ m (a) the new rope (b) the worked rope.

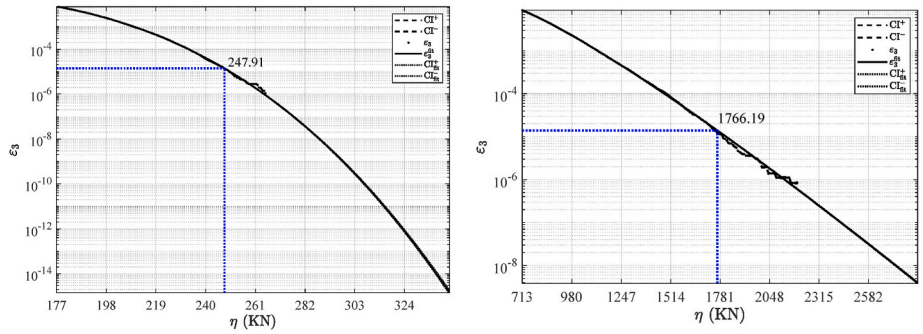

Fig. 12. ACER ε_3 for #1 mooring tension, $R = 81$ m (a) the new rope (b) the worked rope.

Table 4
Extreme mooring tension under different current conditions, unit: KN.

	$R = 77$ m		$R = 81$ m	
EA	Gumbel	ACER	Gumbel	ACER
New	223.55	224.06	247.38	247.91
Worked	1361.34	1382.63	1752.63	1766.19

and the influence of current velocity on motion responses of floating structures reduces with the increase of restoring force of mooring systems. It is also observed that the pretension shows a considerable influence on extreme mooring tension, i.e., the extreme mooring tension increases with the pretension. The reason is that a small movement of a floating structure will induce great mooring tension for taut mooring, especially for moorings operate in shallow water.

4.2.3. Influence of tidal range on short-term extreme mooring tensions

The water depth at offshore locations is time variable due to tides, wind and atmospheric pressure. The contribution of tides on the variations of water depth in shallow water is much greater than that of deep water. Consequently, the influence of tides on extreme mooring tension needs to be investigated for shallow-water floating structures. In this study, six tides cases are discussed for each mooring pretension, and there are three mooring pretension cases studied ($R = 81$, 85 and 90 m). The influence of tides on system dynamics is considered by adjusting the water depth, for instance, the water depth is changed from 84.12 m (the original water depth) to 84.22 m when the tide elevation is 0.1 m. The mooring tensions under different tidal conditions are summarized in Table 6. The variation of the draft of the WEC due to tides is limited, and will not be taken into account in this study.

Mooring tension time series under different tidal ranges when $R = 81$ m are plotted in Fig. 16, where T_i denotes the tide elevation and it is seen that the influence of tide elevation on mooring tension is limited, especially when the tide elevation is small.

The numerical simulations of each case are then repeated fifty times for extreme mooring tension analysis, and the maximum tension of each simulation is considered as the sample of Gumbel distribution. The Q-Q plots of Gumbel model of extreme mooring tension under $T_i = 1$ m for different mooring radii are shown in Fig. 17, where it is observed that the sampled data are well distributed along the reference line. It indicates that the parameters of Gumbel model are well fitted. The averaged conditional exceedance rates of mooring tensions (cases of $T_i = 1$ m) based on fifty simulations are then fitted by ACER approach and results are plotted in Fig. 18, and it is seen that the ACER method shows good performance in fitting the exceedance rate.

The extreme mooring tensions estimated by Gumbel and ACER method for these studied cases are summarized in Table 7, where it is seen that the results of ACER method are close to that of Gumbel. It implies that the ACER method presents accurate enough estimations of extreme mooring tensions. The influence of tides on extreme mooring tension increases with tidal range since the variation of mooring

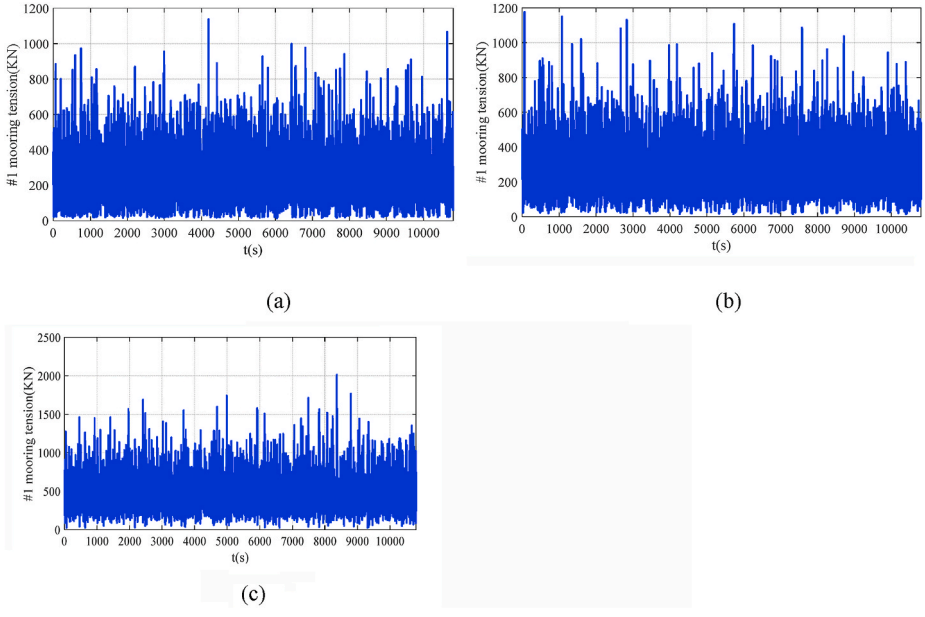

Fig. 13. #1 Mooring tension time series, $R = 77$ m (a) $V_{c0} = 0$ m/s (b) $V_{c0} = 0.5$ m/s (c) $V_{c0} = 2$ m/s.

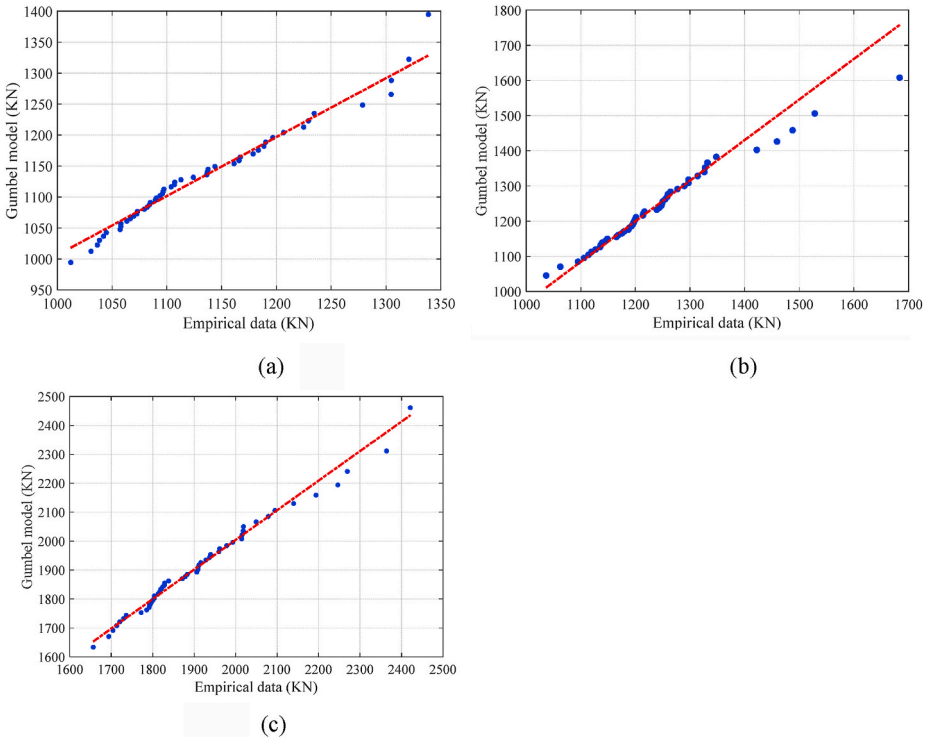

Fig. 14. Q-Q plot of Gumbel model for extreme tension analysis of #1 mooring, $R = 77$ m (a) $V_{c0} = 0$ m/s (b) $V_{c0} = 0.5$ m/s (c) $V_{c0} = 2$ m/s.

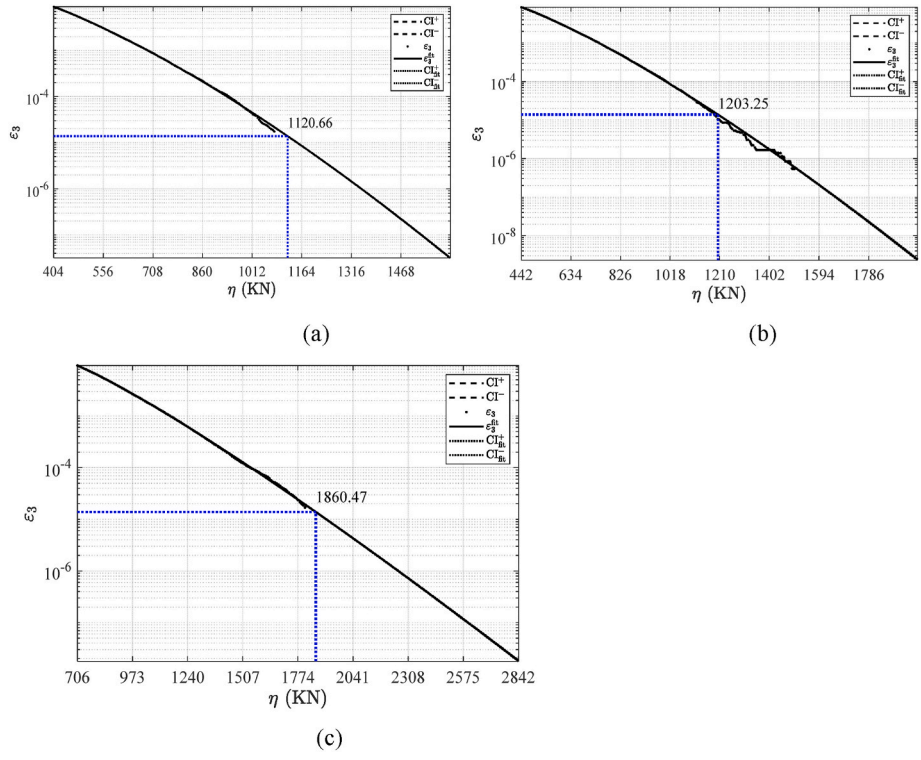

Fig. 15. ACER ε_3 for #1 mooring tension, $R = 77$ m (a) $V_{c0} = 0$ m/s (b) $V_{c0} = 0.5$ m/s (c) $V_{c0} = 2$ m/s.

pretension increases with tide elevation. For cases with a small tidal range ($\pm 0.1, \pm 0.4m$), the influence of tides on extreme mooring tension is ignorable. The extreme mooring tension when $T_i = 1\ m$ is around 12% greater than that when $T_i = -1\ m$ for all studied pretension cases.

4.2.4. *Influence of time duration and number of simulations on the performance of ACER method for extreme mooring tension analysis based on extrapolation approach*

In the previous discussion, the 3-h short-term extreme mooring tension is studied by fifty 3-h fully coupled dynamic analyses, e.g., the analysis is inefficient. In this section, the extrapolation approach based

Table 5
Extreme mooring tension under different current conditions, unit: KN.

	$R = 77$ m		$R = 81$ m		$R = 85$ m	
V_c(m/s)	Gumbel	ACER	Gumbel	ACER	Gumbel	ACER
0.00	1094.35	1120.66	1510.13	1544.43	1960.12	1976.68
0.50	1185.30	1203.25	1585.42	1611.37	2125.02	2123.43
2.00	1839.60	1860.47	2181.52	2200.96	2586.06	2577.43

Table 6
Mooring pretension under different current conditions, unit: KN.

Tides(m)	$R = 81$ m	$R = 85$ m	$R = 90$ m
0.10	378	624	1082
−0.10	366	606	1060
0.40	394	645	1117
−0.40	351	584	1029
1.00	428	694	1179
−1.00	319	543	969

on ACER is applied to study the extreme mooring tension, and the results of the Gumbel method are acted as reference values to check the accuracy of the extrapolation approach. The implementation of the extrapolation method can be found in Eqs. (21)–(24).

The extreme tensions of #1 mooring estimated by extrapolation method under different pretensions when $V_{c0} = 0.5$ m are plotted in Fig. 19. To study the influence of the time duration and the number of simulations on the performance of extrapolation method based on ACER in extreme mooring tension analysis, two-time durations (20 and 30 min) are discussed with several simulations varies from 8 to 40. The extreme mooring tensions estimated by the Gumbel method based on fifty 3-h fully coupled analyses acted as benchmarks to check the accuracy of the extrapolation approach. It is observed that both the number of simulations and time durations show some influences on estimated extreme mooring tension by the extrapolation method. It is seen that there are great variations in extreme mooring tension when the number of simulations is small, which implies that it will introduce great uncertainties in extreme mooring tension analysis by extrapolation method for these cases.

However, it is seen that the estimated extreme mooring tension tends to be stable with the increase in the number of simulations, and the number of simulations needed to obtain stable results decreases with the increase of pretension. It is explained that the influence of random wave elevations on floating system dynamics reduces with the increase of pretension since the mooring system restoring force increases with pretension. The extrapolation method overestimates extreme mooring tension in most cases, especially when the pretension is small and 20 min of data are used. Furthermore, estimated extreme mooring tensions based on 30 min of data are more accurate than results estimated through 20 min of data in most studied cases.

The extreme tensions of #1 mooring estimated by extrapolation method under different pretensions when $V_{c0} = 2$ m are plotted in Fig. 20. If compare results in Fig. 20 with that in Fig. 19, it is found that the number of simulations needed to obtain stable results increases with the current velocity. The reason is that nonlinearities of mooring tension increase with current velocity. The extrapolation method slightly

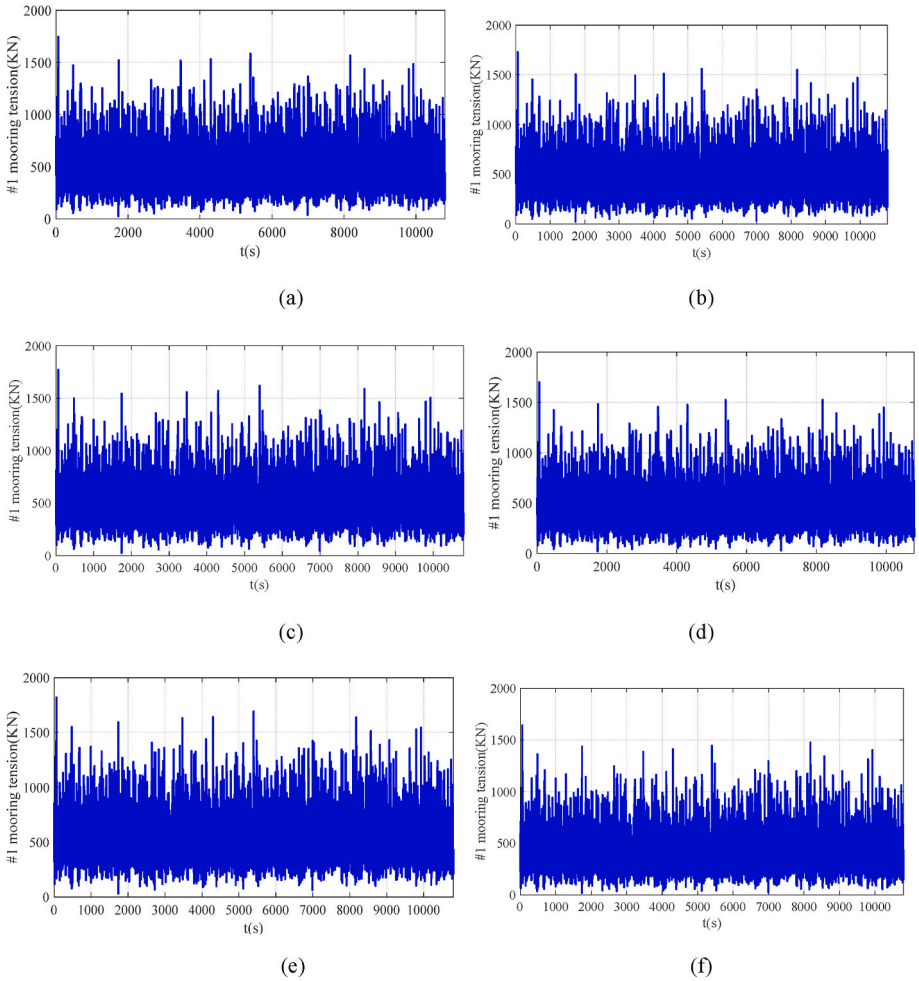

Fig. 16. #1 Mooring tension time series, $R = 81$(m) (a) $T_i = 0.1$ m (b) $T_i = -0.1$ m (c) $T_i = 0.4$ m (d) $T_i = -0.4$ m(e) $T_i = 1$ m (f) $T_i = -1$ m.

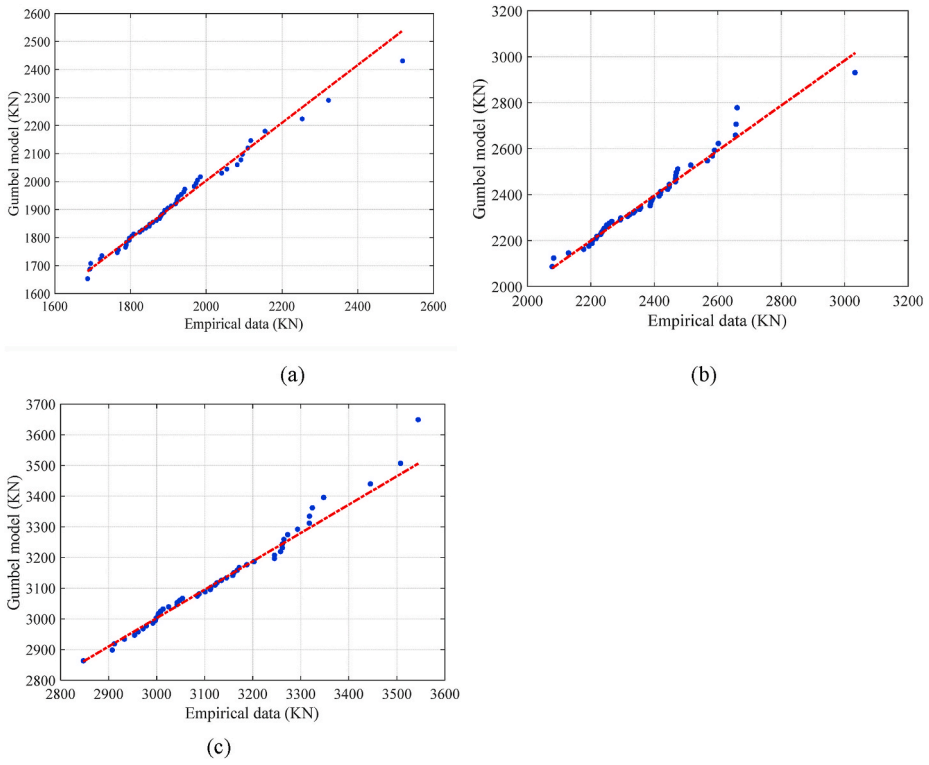

Fig. 17. Q-Q plot of Gumbel model for extreme tension analysis of #1 mooring, $T_i = 1$ m (a) $R = 81m$ (b) $R = 85m$ (c) $R = 90m$.

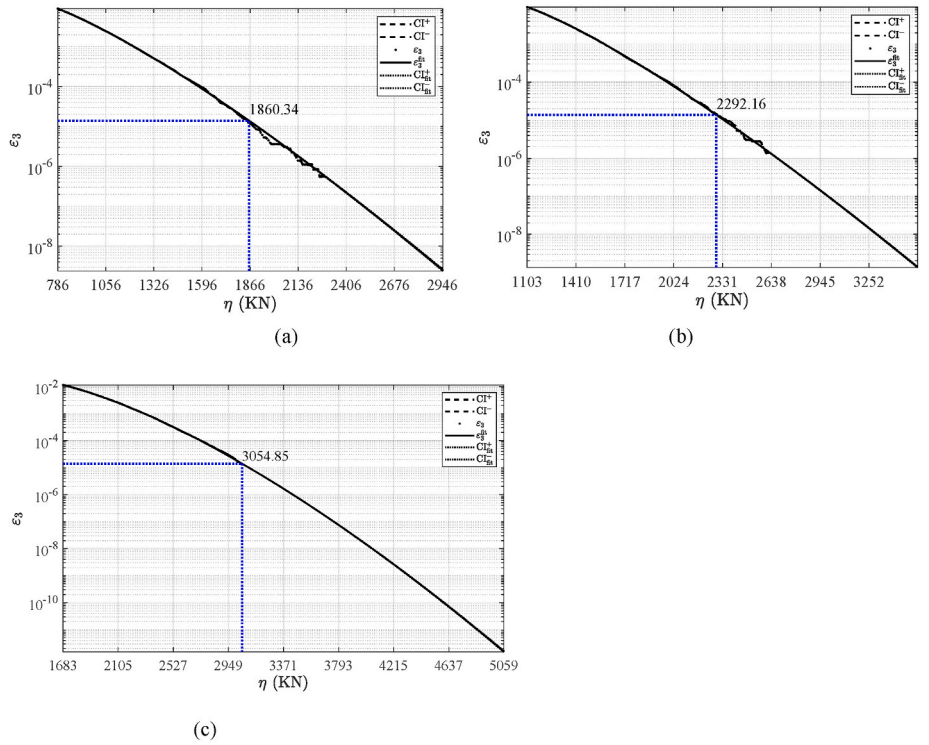

Fig. 18. ACER ε_3 for #1 mooring tension, $T_i = 1$ m (a) $R = 81m$ (b) $R = 85m$ (c) $R = 90$ m.

overestimates extreme mooring tension in most cases, and the results estimated based on 30 min of data are slightly smaller than that estimated based on 20 min of data. However, the extrapolation method can present precise enough estimations of the extreme mooring tension when the number of simulations is large enough.

5. Conclusions

Both the experimental tests and numerical simulations are applied to study the dynamics of a floating WEC moored by nylon mooring lines. The comparisons between numerical simulations and model test results

Table 7
ACER ε_3 for #1 mooring tension, $T_i = 2$ m (a) $R = 81m$ (b) $R = 85m$ (c) $R = 90m$, unit: KN.

Tidal (m)	$R = 81$ m		$R = 85$ m		$R = 90$ m	
	Gumbel	ACER	Gumbel	ACER	Gumbel	ACER
0.10	1762.46	1775.97	2187.81	2181.93	2905.18	2900.23
−0.10	1742.87	1755.11	2163.64	2157.46	2871.57	2865.03
0.40	1791.24	1805.94	2224.06	2217.50	2956.14	2953.66
−0.40	1713.06	1723.42	2127.39	2122.49	2819.90	2810.66
1.00	1846.88	1860.34	2297.08	2292.16	3059.58	3054.85
−1.00	1651.49	1658.17	2055.93	2054.26	2715.71	2708.30

indicate that the numerical method can accurately predict the maximum mooring tensions.

The influence of mooring axial stiffness, current velocity and tidal range on extreme mooring tension analysis is conducted by the calibrated numerical model, and it has been shown that the ACER method presents accurate estimations of extreme mooring tension based on fifty 3-h simulations. There is a great difference between the axial stiffness of new and worked nylon rope. The extreme mooring tension of the worked rope is several times that of the new rope, and the difference between these two values increases with the mooring pretension. It indicates that obtaining the axial stiffness of worked ropes is essential in mooring design, otherwise, the extreme mooring tension will be underestimated dramatically if the axial stiffness of new ropes is used. The extreme

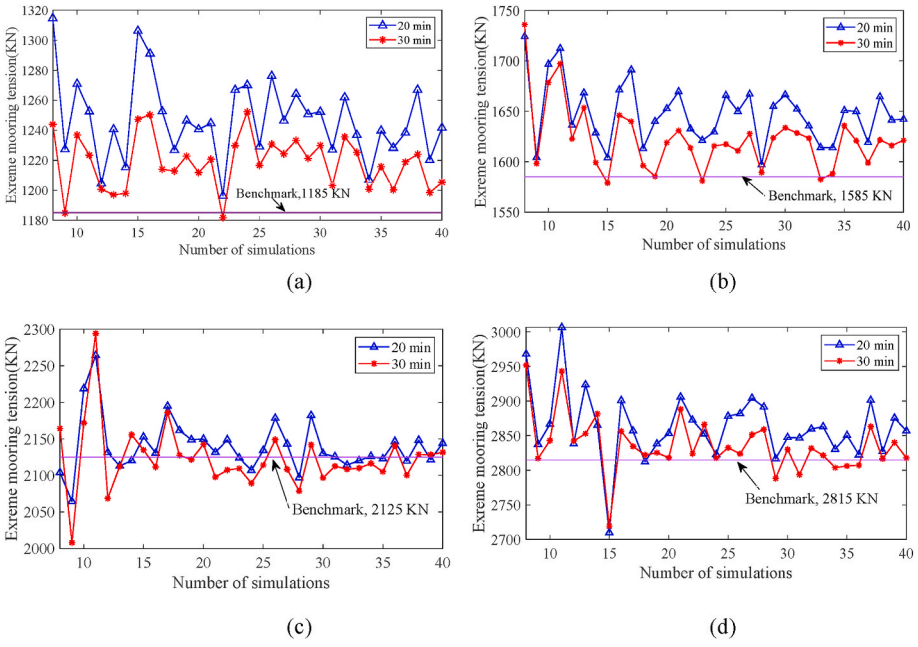

Fig. 19. Estimated extreme tension of #1 mooring by extrapolation method, $V_{c0} = 0.5$ *m* (a) $R = 77$ *m* (b) $R = 81$ *m* (c) $R = 85$ *m* (d) $R = 90$ *m*.

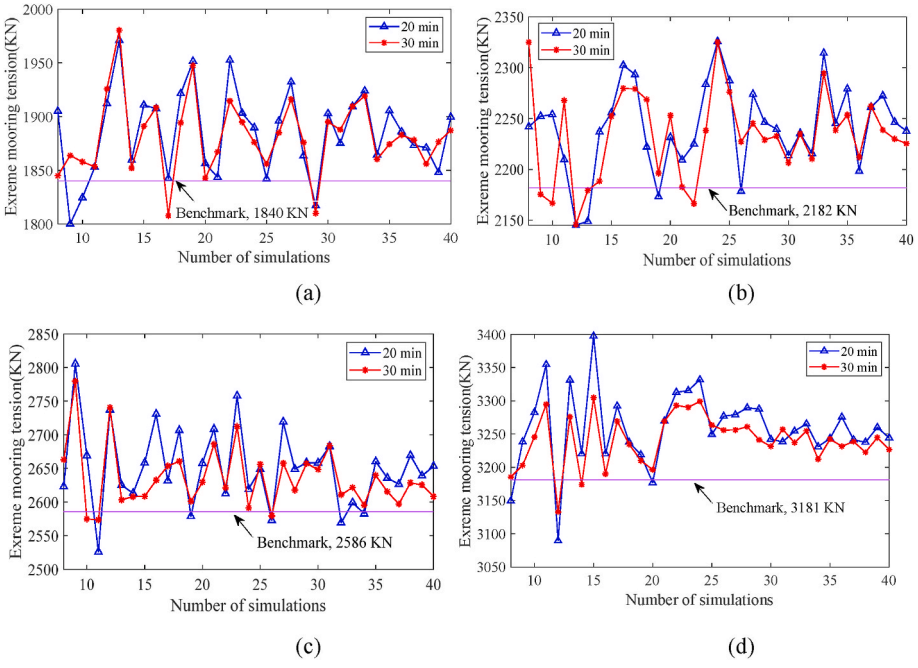

Fig. 20. Estimated extreme tension of #1 mooring by extrapolation method, $V_{c0} = 2$ *m* (a) $R = 77$ *m* (b) $R = 81m$ (c) $R = 85m$ (d) $R = 90$ *m*.

mooring tension increases with current velocity, and the influence of current velocity on the extreme mooring tension reduces with the increase of mooring pretension. The influence of tides should be taken into consideration in the mooring design process if the water depth of the target field is small but with a great tidal elevation, otherwise, the failure risk of mooring and anchoring will be increased.

The ACER method based on fifty 3-h simulations can present good estimations of extreme mooring tensions. However, this method is less efficient. The extrapolation method which adopts thirty-five 20 min based on ACER is suggested for the extreme mooring tension method, which is much more efficient and accurate enough.

CRediT authorship contribution statement

Sheng Xu: Methodology, Formal analysis, Visualization, Writing – original draft. **C. Guedes Soares:** Conceptualization, Supervision, Writing – review & editing.

Declaration of competing interest

The authors declare that they have no known competing financial interests or personal relationships that could have appeared to influence the work reported in this paper.

Data availability

No data was used for the research described in the article.

Acknowledgement

This work was financially supported by the Project "ELASTMOOR - Elastic mooring systems for wave energy converters" which is co-funded by European Union's Horizon 2020research and innovation programme under the framework of OCEANERA-NET (http://oceaneranet.eu) and by the Portuguese Foundation for Science and Technology (Fundação para a Ciência e Tecnologia - FCT) under contract (OCEANERA/0006/2016). The first author is supported by the Jiangsu Provincial Natural Science Foundation (grant number BK20220653). The work contributes to the Strategic Research Plan of the Centre for Marine Technology and Ocean Engineering (CENTEC), which is financed by the Portuguese Foundation for Science and Technology (Fundação para a Ciência e Tecnologia - FCT) under contract UIDB/UIDP/00134/2020.

References

Ahamed, R., McKee, K., Howard, I., 2020. Advancements of wave energy converters based on power take off (PTO) systems: a review. Ocean Eng. 204, 107248.
Ambühl, S., Sterndorff, M., Sørensen, J.D., 2014. Extrapolation of extreme response for different mooring line systems of floating wave energy converters. Int. J. Mar. Energy 7, 1–19.
ANSYS Inc, 2015. ANSYS AQWA Users Manual.
Arena, F., Romolo, A., Malara, G., Fiamma, V., Laface, V., 2017. The first full operative U-owc plants in the port of civitavecchia. In: Proceedings of the International Conference on Offshore Mechanics and Arctic Engineering - OMAE. American Society of Mechanical Engineers Digital Collection. OMAE2017-62036, V010T09A022.
Bhinder, M.A., Karimirad, M., Weller, S., Debruyne, Y., Guérinel, M., Sheng, W.A., 2015. Modelling mooring line non-linearities (material and geometric effects) for a wave energy converter using AQWA, SIMA and Orcaflex. In: 11th European Wave and Tidal Energy Conference. Nantes, France.
Bílková, D., 2014. Robust parameter estimations using L-moments, TL-moments and the order statistics. Am. J. Appl. Math. 2, 36.
Castro-Santos, L., Martins, E., Guedes Soares, C., 2016. Methodology to calculate the costs of a floating offshore renewable energy farm. Energies 9 (5), 324–350.
Cheng, Z., Madsen, H.A., Chai, W., Gao, Z., Moan, T., 2017. A comparison of extreme structural responses and fatigue damage of semi-submersible type floating horizontal and vertical axis wind turbines. Renew. Energy 108, 207–219.
Clément, A., McCullen, P., Falcão, A., Fiorentino, A., Gardner, F., Hammarlund, K., Lemonis, G., Lewis, T., Nielsen, K., Petroncini, S., Pontes, M.-T., Schild, P., Sjöström, B.-O., Sørensen, H.C., Thorpe, T., 2002. Wave energy in Europe: current status and perspectives. Renew. Sustain. Energy Rev. 6, 405–431.
Czech, B., Bauer, P., 2012. Wave energy converter concepts: design challenges and classification. IEEE Ind. Electron. Magaz. 6, 4–16.
Depalo, F., Wang, S., Xu, S., Guedes Soares, C., Yang, S.-H., Ringsberg, J.W., 2022. Effects of dynamic axial stiffness of elastic moorings for a wave energy converter. Ocean Eng. 251, 111132.
Diaz, H.M., Guedes Soares, C., 2020. Review of the current status, technology and future trends of offshore wind farms. Ocean Eng., 209107381
Dnv, G.L., 2017. Environmental Conditions and Environmental Loads. DNVGL-RP-C205.
Drew, B., Plummer, A.R., Sahinkaya, M.N., 2009. A review of wave energy converter technology. Proc. IME J. Power Energy 223, 887–902.
Elginoz, N., Bas, B., 2017. Life Cycle Assessment of a multi-use offshore platform: combining wind and wave energy production. Ocean Eng. 145, 430–443.
de Falcão, A.F.O., 2010. Wave energy utilization: a review of the technologies. Renew. Sustain. Energy Rev. 14, 899–918.
Falnes, J., 2007. A review of wave-energy extraction. Mar. Struct. 20, 185–201.
Fitzgerald, J., 2009. Position Mooring of Wave Energy Converters. Ph.D. thesis. Chalmers University of Technology.
Gaspar, J.F., Calvario, M., Kamarlouei, M., Guedes Soares, C., 2016. Power Take-Off Concept for Wave Energy Converters Based on Oil-Hydraulic Transformer Units. Renewable Energy, pp. 861232–861246.
Gaspar, J.F., Kamarlouei, M., Thiebaut, F., Guedes Soares, C., 2021. Compensation of a hybrid platform dynamics using wave energy converters in different sea state conditions. Renew. Energy 177, 871–883.
Gielen, D., Boshell, F., Saygin, D., Bazilian, M.D., Wagner, N., Gorini, R., 2019. The role of renewable energy in the global energy transformation. Energy Strategy Rev. 24, 38–50.
Guedes Soares, C., Bhattacharjee, J., Tello, M., Pietra, L., 2012. In: Garbatov Y, C., Sutulo, S., Santos, T.A. (Eds.), Review and Classification of Wave Energy Converters. Guedes Soares, Maritime Engineering and Technology. UK Taylor & Francis Group, London, pp. 585–594.
Kamarlouei, M., Gaspar, J.F., Guedes Soares, C., 2022. Optimal design of an axisymmetric two-body wave energy converter with translational hydraulic power take-off system. Renew. Energy 183586–183600.
Kim, J.-S., Nam, B.W., Park, S., Kim, K.-H., Shin, S.-H., Hong, K., 2022. Numerical investigation on hydrodynamic energy conversion performance of breakwater-integrated oscillating water column-wave energy converters. Ocean Eng. 253, 111287.
Kong, F., Su, W., Liu, H., Collu, M., Lin, Z., Chen, H., Zheng, X., 2019. Investigation on PTO control of a combined axisymmetric buoy-WEC(CAB-WEC). Ocean Eng. 188, 106245.
Lankhorst Offshore. Double braid 32/64. URL, 8.2.21. https://www.lankhorstoffshore.com/products/double-braid-32/64.
Li, C.B., Choung, J., 2021. Effects of strain- and strain rate- dependent nonlinear mooring line stiffness on floating platform motion. Ocean Eng. 241, 110011.
Li, M., Wu, R., Wu, B., Yang, Z., Li, G., 2022. Hydrodynamic performance and optimization of a pneumatic type spar buoy wave energy converter. Ocean Eng. 254, 111334.
Liu, H., Huang, W., Lian, Y., Li, L., 2014. An experimental investigation on nonlinear behaviors of synthetic fiber ropes for deepwater moorings under cyclic loading. Appl. Ocean Res. 45, 22–32.
López, I., Andreu, J., Ceballos, S., Martínez de Alegría, I., Kortabarria, I., 2013. Review of wave energy technologies and the necessary power-equipment. Renew. Sustain. Energy Rev. 27, 413–434.
Naess, A., Gaidai, O., 2009. Estimation of extreme values from sampled time series. Struct. Saf. 31, 325–334.
Nguyen, H.P., Wang, C.M., Tay, Z.Y., Luong, V.H., 2020. Wave energy converter and large floating platform integration: a review. Ocean Eng. 213, 107768.
Ochi, M.K., 1981. Principles of extreme value statistics and their application. In: Extreme Loads Response Symposium. SNAME, Arlington, VA, pp. 15–30.
Pham, H.-D., Cartraud, P., Schoefs, F., Soulard, T., Berhault, C., 2019. Dynamic modeling of nylon mooring lines for a floating wind turbine. Appl. Ocean Res. 87, 1–8, 3.
Pickands, J., 1975. Statistical inference using extreme order statistics. Ann. Stat. 3, 119–131.
Razola, M., Olausson, K., Garme, K., Rosén, A., 2016. On high-speed craft acceleration statistics. Ocean Eng. 114, 115–133.
Rezanejad, K., Bhattacharjee, J., Guedes Soares, C., 2015. Analytical and numerical study of dual-chamber oscillating water columns on stepped bottom. Renew. Energy 75272–75282.
Saha, N., Gao, Z., Moan, T., Naess, A., 2014. Short-term extreme response analysis of a jacket supporting an offshore wind turbine. Wind Energy 17, 87–104.
Sahu, A., Yadav, N., Sudhakar, K., 2016. Floating photovoltaic power plant: a review. Renew. Sustain. Energy Rev. 66, 815–824.
Schubert, B.W., Robertson, W.S.P., Cazzolato, B.S., Sergiienko, N.Y., Ghayesh, M.H., 2022. Nonlinear stiffness enhancement of submerged wave energy device in high fidelity model. Ocean Eng. 254, 111295.
Sheng, W., 2019. Wave energy conversion and hydrodynamics modelling technologies: a review. Renew. Sustain. Energy Rev. 109, 482–498.
Shih, R.-S., Liu, Y.-C., 2022. Experimental study on the optimization of an oscillating water column structure considering real gas compressibility. Ocean Eng. 254, 111356.
Stanisic, D., Efthymiou, M., Kimiaei, M., Zhao, W., 2018. Design loads and long term distribution of mooring line response of a large weathervaning vessel in a tropical cyclone environment. Mar. Struct. 61, 361–380.
Tan, J., Polinder, H., Laguna, A.J., Miedema, S., 2022. A numerical study on the performance of the point absorber Wave Energy Converter integrated with an adjustable draft system. Ocean Eng. 254, 111347.

Thorpe, T.W., 1999. A Brief Review of Wave Energy. Technical report ETSU-R120 200.
Xu, S., Guedes Soares, C., 2021a. Bayesian analysis of short term extreme mooring tension for a point absorber with mixture of Gamma and Generalised Pareto distributions. Appl. Ocean Res. 102556.
Xu, S., Guedes Soares, C., 2021b. Evaluation of spectral methods for long term fatigue damage analysis of synthetic fibre mooring ropes based on experimental data. Ocean Eng. 226, 108842.
Xu, S., Guedes Soares, C., 2020. Experimental investigation on short-term fatigue damage of slack and hybrid mooring for wave energy converters. Ocean Eng. 195, 106618.
Xu, S., Ji, C., Guedes Soares, C., 2019a. Estimation of short-term extreme responses of a semi-submersible moored by two hybrid mooring systems. Ocean Eng. 190, 106388.
Xu, S., Ji, C. yan, Guedes Soares, C., 2021a. Short-term extreme mooring tension and uncertainty analysis by a modified ACER method with adaptive Markov chain Monte Carlo simulations. Ocean Eng. 236, 109445.
Xu, S., Wang, S., Guedes Soares, C., 2021b. Experimental investigation on the influence of hybrid mooring system configuration and mooring material on the hydrodynamic performance of a point absorber. Ocean Eng. 223, 109178.
Xu, S., Wang, S., Guedes Soares, C., 2021c. Experimental study of the influence of the rope material on mooring fatigue damage and point absorber response. Ocean Eng. 232, 108667.
Xu, S., Wang, S., Guedes Soares, C., 2021d. Experimental study of the influence of the rope material on mooring fatigue damage and point absorber response. Ocean Eng. 232, 108667.
Xu, S., Wang, S., Guedes Soares, C., 2020. Experimental investigation on hybrid mooring systems for wave energy converters. Renew. Energy 158, 130–153.
Xu, S., Wang, S., Guedes Soares, C., 2019b. Review of mooring design for floating wave energy converters. Renew. Sustain. Energy Rev. 111, 595–621.
Xu, S., Wang, S., Liu, H., Zhang, Y., Li, L., Guedes Soares, C., 2021e. Experimental evaluation of the dynamic stiffness of synthetic fibre mooring ropes. Appl. Ocean Res. 112, 102709.
Yang, S.H., Ringsberg, J.W., Johnson, E., Hu, Z., 2020. Experimental and numerical investigation of a taut-moored wave energy converter: a validation of simulated mooring line forces. Ships Offshore Struct. 1–15.
Yang, S.H., Ringsberg, J.W., Johnson, E., Hu, Z., Bergdahl, L., Duan, F., 2018. Experimental and numerical investigation of a taut-moored wave energy converter: a validation of simulated buoy motions. Proc. IME M J. Eng. Marit. Environ. 232, 97–115.
Zhao, X.L., Ning, D.Z., Zou, Q.P., Qiao, D.S., Cai, S.Q., 2019. Hybrid floating breakwater-WEC system: a review. Ocean Eng. 186, 106126.
Zhao, Y., Liao, Z., Dong, S., 2021. Estimation of characteristic extreme response for mooring system in a complex ocean environment. Ocean Eng. 225, 108809.